Nano Energy 44 (2018) 228–239

Contents lists available at ScienceDirect

Nano Energy

journal homepage: www.elsevier.com/locate/nanoen

Full paper

Layer-by-layer assembly-induced triboelectric nanogenerators with high and stable electric outputs in humid environments

Dojin Kim[1], Seokmin Lee[1], Yongmin Ko, Cheong Hoon Kwon, Jinhan Cho*

Department of Chemical and Biological Engineering, Korea University, Anam-dong, Seongbuk-gu, Seoul 136-713, South Korea

ARTICLE INFO

Keywords:
Triboelectric nanogenerator
Layer-by-Layer assembly
Nano-/micro-structure
Fluorination, Humidity

ABSTRACT

We introduce a layer-by-layer (LbL) assembly-induced triboelectric nanogenerator (TENG) with a high and stable electric output under a wide range of humidity conditions. In this study, highly porous (cationic poly (allylamine hydrochloride) (PAH)/anionic poly(acrylic acid) (PAA))$_n$ multilayer films were prepared via a pH-controlled electrostatic LbL assembly with a subsequent acid treatment and were used as a mold for the triboelectric poly(dimethylsiloxane) (PDMS) replica. The electrical output of the TENGs composed of a protuberant PDMS plate and Al electrodes significantly increased based on the evolution of the nano-/micro-structured PDMS bumps. Particularly, the protuberant PDMS film molded from the porous (1.5 mg mL^{-1} PAH/0.5 mg mL^{-1} PAA)$_{20}$ multilayers displayed a high open-circuit voltage output of 242 V and a short-circuit current density of 16.2 μA cm^{-2} under a compressive force of 90 N in a relative humidity (RH) of 20%. When this hierarchical PDMS surface was additionally modified by fluorine self-assembled monolayer, the voltage output and current density of the resultant TENG at the same experimental conditions were increased up to approximately 288 V and 17 μA cm^{-2}, respectively, exhibiting a remarkably high humidity-resistant electrical performance (16% loss of the initial voltage at 80% RH).

1. Introduction

Triboelectric nanogenerators (TENGs), which convert mechanical energy into electricity using the triboelectric effect coupled with electrostatic effects, have attracted considerable attention due to their simple and cost-effective device structures and substantial usefulness as a sustainable and renewable energy source for a variety of self-powered and mobile electronics [1–12]. Generally, the charge generation and transfer (i.e., current flow) in a triboelectric process are caused by periodic contact/separation between two materials with different triboelectric polarities. Therefore, a higher difference in the triboelectric polarities and a larger triboelectric surface area for charge generation induce a higher electric output under the same applied force [4,13–16]. More specifically, in the case of TENGs composed of Al electrodes and poly(dimethylsiloxane) (PDMS) plates, which have a high difference in their reciprocal triboelectric polarities, the introduction of nanomaterials and/or creation of bumpy or porous surface morphologies on the triboelectric films using natural mold [17] or a variety of self-assembly processes (e.g., nanoparticle or nanowire self-assembly or selective etching of spontaneous block copolymer templates) can significantly increase the electric output of TENGs compared to that of the flat triboelectric film-based TENGs [17–26]. However, their electric output performance tends to rapidly degrade indicating the dissipation of triboelectric surface charges in highly humid environments, which is a critical obstacle to their practical and commercial applications.

Recently, Nguyen et al. reported the effect of relative humidity (RH) on micropatterned PDMS-based TENGs [27], and additionally they elucidated that the formation of a water skin layer on the triboelectric plates induced the charge transfer or dissipation. For resolving such a humidity-related drawback of TENGs, various attempts have been made to create triboelectric films that mimic a superhydrophobic surface (water contact angle > 150°) with hierarchical dual-sized roughness (i.e., nano/micro-sized roughness) and low surface energy to effectively obstruct the formation of a water skin layer (or droplet) onto the film surface [17,28,29]. Furthermore, the size and shape of the PDMS features can cause notable capacitance changes under a compressive force and resultantly have a significant effect on the electric output performance [29]. However, in many cases, such TENGs require high-cost, complex, and elaborate structural designs and multi-replica processes to create the dual-sized protuberant structures similar to superhydrophobic surfaces, which partially negate the abovementioned advantages of TENGs [24]. For example, in the case of natural molds such

* Corresponding author.
E-mail address: jinhan71@korea.ac.kr (J. Cho).
[1] These authors equally contribute to this work.

https://doi.org/10.1016/j.nanoen.2017.12.001
Received 28 August 2017; Received in revised form 1 December 2017; Accepted 1 December 2017
Available online 07 December 2017

as lotus leaf, rose petal, or cicada wing, although highly protuberant PDMS can be prepared through multi-replica process, the protuberances formed onto PDMS are not dual-sized but nano- or micro-sized structures, and additionally the area of PDMS plates is determined by the size of natural mold [17,30]. Therefore, a more general and facile strategy for the preparation of triboelectric films with a hierarchical surface roughness on a dual-size scale has been strongly needed for high-performance TENGs with humidity-resistant properties.

A LbL assembly based on complementary interactions (i.e., electrostatic, hydrogen-bonding, or covalent interactions) between constituent species is potentially the most versatile process for preparing polymer nanocomposite films with a controlled thickness, composition, and functionality on various substrates, irrespective of the substrate size or shape [31–37]. Particularly, LbL assembly is advantageous for the fabrication of highly porous thick film templates. Rubner et al. reported that weak polyelectrolyte (PE) (i.e., PE with a pH-dependent charge density) multilayers with large quantities of entangled PE chains under specific pH conditions could be easily converted into porous films via additional acid treatment [38,39]. More specifically, weak PE multilayers composed of cationic amine ($-NH_3^+$) group-functionalized poly (allylamine hydrochloride) (PAH) and anionic carboxylic acid ($-COO^-$) group-functionalized poly(acrylic acid) (PAA) can form the thickest film at pH 7.5 for PAH and at pH 3.5 for PAA, and the films can be converted into highly porous films after exposure to acidic conditions (pH $\leq$ 2.5) due to the dissociation and rearrangement of the electrostatic bonds formed within the PE multilayers. Therefore, if the porosities of these LbL-assembled films can be controlled and the resultant films can be used as a mold for PDMS films, this approach may allow the fabrication of humidity-resistant TENGs via the formation of triboelectric films with hierarchical surface morphologies.

Here, we introduce a LbL assembly-induced TENG that exhibits a high electric output under a wide range of humidity conditions using a replica of nano/microporous PE multilayer films. Our approach is characterized by the fact that the nano-/micro-sized triboelectric features are directly prepared through one time-replica process, and additionally fused into an all-in-one PDMS, resulting in an enhanced hydrophobicity as well as the mechanically stable properties. Furthermore, we highlight that these triboelectric films with dual-sized and fluorinated PDMS features can increase the triboelectric surface area including electrostatic-induction area, and additionally cause capacitance changes under a periodic compressive force, which have a notable effect on the improvement in the electric output performance. For this study, the (cationic poly(allylamine hydrochloride) (PAH)/anionic poly(acrylic acid) (PAH))$_n$ multilayer films were prepared using an electrostatic LbL-assembly, and then, the films were sequentially dipped in acidic water for the formation of nano-/micro-porous multilayers. The porosity of the multilayers was controlled by the solution concentration of the PEs (for the multilayer deposition) and the solution pH (for the acidic treatment). When the porous PE multilayers were used as the mold for the preparation of triboelectric PDMS films, the replicated PDMS films exhibited enhanced hydrophobic properties due to the formation of the nano-/micro-structured bumps and the relatively low surface energy of the PDMS. These film devices (1.5 cm $\times$ 1.5 cm for the PDMS and 3 cm $\times$ 3 cm for the Al electrode) displayed a high electric output of 242 V and 16 μA cm^{-2} (for comparison, the electric output of a flat PDMS film is $\sim$ 75 V and 6.1 μA cm^{-2}) under a compressive force of 90 N at 20% RH, and the output voltage retained 194 V (in comparison, the output voltage of a flat PDMS film is $\sim$ 14 V) under a high humidity condition of 80% RH. Additionally, when this hierarchical PDMS surface was modified by fluorine-functionalized organics (1H, 1H, 2H, 2H-perfluorooctyltrichlorosilane (FOTS)) with extremely low surface energy, the formed PDMS films exhibited a high degree of water repellant properties (water contact angle $\sim$ 148°) shown in superhydrophobic surface, inducing higher electronegative property. Particularly, the electric output of fluorinated PDMS-based device were further increased up to approximately 288 V and 17 μA cm^{-2}, exhibiting long-term cycling stability ($\sim$ 18,000 cycles) under a compressive force of 90 N at 20% RH, respectively. We also highlight that the electric performance of TENGs with all-in-one, dual-sized, and fluorinated PDMS structures exhibited 84% (i.e., 242 V and 14.3 μA cm^{-2}) of initial output at 80% RH. Given that the surface morphology and modification of triboelectric films can be easily and delicately controlled using an electrostatic LbL assembly and additional fluorination treatment, our approach can provide a facile, versatile and cost-effective tool for designing large-area TENGs with a notable electric output and high humidity-resistant performance.

2. Experimental section

2.1. Materials

Polyelectroytes (i.e., poly(allyamine hydrochloride) (PAH) and poly (acrylic acid) (PAA)) and dimethylsiloxane, PDMS (Sylgard 184) were purchased from Alfa Aesar, Sigma-Aldrich, and Dow Corning, respectively.

2.2. Preparation of the porous PE multilayers

The solution concentration of PAH (M_w = 120,000–200,000) was fixed at 1.5 mg mL^{-1} at pH 7.5, and the aqueous solution of PAA (M_w = 130,000) were prepared at concentrations of 0.5, 1.0, 1.5, and 2.0 mg mL^{-1} at pH 3.5. For the build-up of the LbL assembled multilayer, the silicon substrates were first cleaned with a base-peroxide solution ($H_2O/NH_4OH/H_2O_2$ 5:1:1 *v/v/v*) at 60 °C. The resulting negatively charged substrates were first dipped into the cationic PAH for 10 min and then, washed twice with deionized water. Then, the PAH-coated substrates were dipped into a PAA solution for 10 min. These dipping processes were repeated until the desired bilayer number was obtained. After that, acidic water was dropped onto the PAH/PAA multilayer-coated substrates for the formation of porous films.

2.3. Preparation of the triboelectric PDMS replica

For the preparation of the PDMS replica films, 1H, 1H, 2H, 2H-perfluorooctyltrichlorosilane (FOTS) was first coated onto the porous multilayer-coated substrates, and the PDMS prepolymer mixture (PDMS prepolymer: cross-linker agent = 10:1, w/w) was subsequently poured onto the porous multilayer templates using a doctor-blade process. This surface treatment allowed a facile incorporation of the PDMS prepolymer into the porous films and additionally the facile detachment of the resultant PDMS replica from the multilayer films. The total thickness of the resultant PDMS replica films prepared using the doctor blade approach was fixed at approximately 500 μm. After this process, the films were thermally cured at 150 °C for 40 min. The cured PDMS films were carefully peeled off of the multilayer-coated substrate. The embossed structure and protuberance size of the triboelectric PDMS replica films were determined by the pore size and shape formed within porous multilayer films.

2.4. Measurements

Vibrational spectra were measured by FTIR spectroscopy (iS10 FT-IR, Thermo Fisher) in the advanced grazing angle (AGA) mode. The sample chamber was purged with nitrogen gas for two hours to eliminate water and CO_2 prior to conducting the FTIR measurement. The acquired raw data was plotted after baseline correction, and the spectrum was smoothed using spectrum-analyzing software (OMNIC, Nicolet). The surface morphologies of the PDMS replica films were investigated by field-emission scanning electron microscopy (FE-SEM) (Hitachi Inc., model S-4800). A pushing tester (Labworks, Inc., model ET-126–1) was used to produce a vertical compressive strain in the TENGs at a distance of 0.4 cm between the 75 μm-thick Al top and

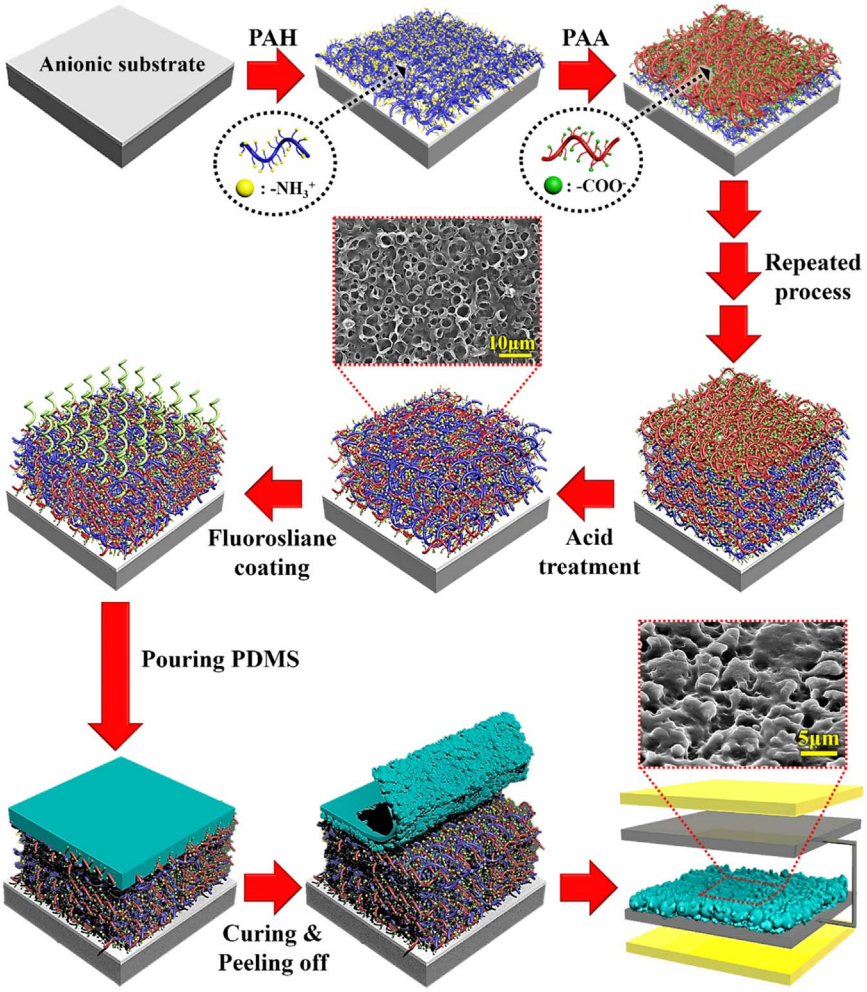

Scheme 1. Schematic for the preparation of triboelectric PDMS films with hierarchically embossed structures using porous PE-multilayered templates.

bottom electrodes (an area of 3 cm × 3 cm). A Tektronix DMO 3052 digital phosphor oscilloscope and a low-noise current preamplifier (Stanford Research Systems, Inc., model SR570) were used to measure the open-circuit output voltage and short-circuit output current, respectively. Water contact angle measurements were performed using Phoenix-300 instrument with Surfaceware 8 (Surface Electro Optics Co., Ltd.). The volume of the water droplet was approximately 7 μL. The potential distribution of the flat and nano-/micro-structured PDMS devices was qualitatively investigated using the COMSOL multiphysics software. Additionally, a nanoindenter (MICRO MATERIALS, NanoTest Vantage Platform) was used to measure the indentation depths and to calculate capacitance from the force-responsive curves.

3. Results and discussion

For the preparation of LbL assembly-induced TENGs with modulated nano-/micro-size protuberances (Scheme 1), the electrostatic LbL-assembled $(PAH/PAA)_n$ nanocomposite multilayers were first prepared by alternately and repeatedly depositing the substrates in the positively charged PAH and negatively charged PAA solutions that were adjusted to pH 7.5 and 3.5, respectively. Generally, the degree of ionization of PAH at pH 7.5 and PAA at pH 3.5 is approximately 80% and 7%, respectively, and the formed LbL-assembled $(pH\ 7.5\ PAH/pH\ 3.5\ PAA)_n$ multilayers exhibited highly entangled PE chain structures with electrostatic and hydrogen-bonding interactions between the PAH and PAA chains [40,41]. As shown in the Fourier transform infrared spectroscopy (FTIR) spectra of the $(pH\ 7.5\ PAH/pH\ 3.5\ PAA)_n$ multilayers (Fig. 1**a**), the intensities of the PAH (asymmetric NH_3^+ bending mode at 1626 cm^{-1} and symmetric NH_3^+ bending at 1517–1523 cm^{-1}) and PAA peaks (asymmetric stretching band of COO^- at 1640, 1542, and 1446 cm^{-1}, and C=O stretching of COOH at 1720 cm^{-1}) regularly increased with the increasing layer number. However, when these LbL-assembled multilayer films were exposed to acidic water (pH < 2.5), the partially charged carboxylic acid (COO^-) groups (at 1640, 1542, and 1446 cm^{-1}) of PAA within multilayers were converted into uncharged carboxylic acid (COOH) groups (at 1720 cm^{-1}) (Fig. 1**b**), which induced the electrostatic bonding dissociation and subsequent chain rearrangement between PAH and PAA within multilayers and resulted in mainly macroporous multilayer films. However, because the porosity of multilayer films is strongly influenced by the degree of PE chain rearrangement due to the acidic treatment, the pore size of the multilayer films can be controlled by the initial concentration of the PE solutions for the LbL deposition.

To confirm these possibilities, we investigated the porosity of the $[pH\ 7.5\ PAH/pH\ 3.5\ PAA]_{20}$ multilayers as a function of the initial PAA solution concentration with a fixed PAH solution concentration (Fig. 2**a**). For this case, the $[1.5\ mg\ mL^{-1}\ PAH/0.5\ mg\ mL^{-1}\ PAA]_{20}$ multilayers after an acid treatment at pH 2.1, exhibited a relatively more uniform nano-/micro-porous structure compared to those of the other multilayer films. Particularly, a number of submicron-sized pores were observed to be embedded within the macropores. Therefore, a decrease in the PAA solution concentration significantly decreased the overall pore size because the excess PAA chains inserted within the multilayers and increased the degree of PE chain rearrangement after the acid treatment, which disturbed the formation of small pores below a submicron size. These results were further confirmed by the pore size

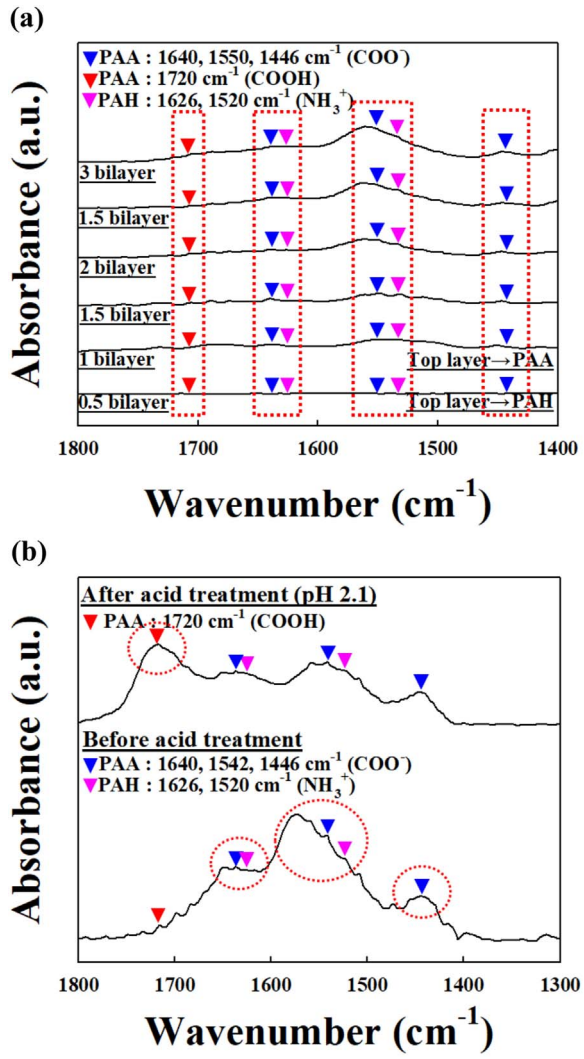

Fig. 1. (a) AGA-FTIR spectra of $[PAH/PAA]_n$ multilayers as a function of the bilayer number. (b) AGA-FTIR spectra of pristine and acid-treated PAH/PAA multilayers during 15 min.

distribution curves measured using the ImageProPlus software program (Fig. 2**b**, Supporting information, Fig. S1).

The porous multilayer films were used as molds for the triboelectric PDMS films with hierarchical surface structure. As shown in Fig. 2**c and d**, the PDMS films, which were replicated from the porous [1.5 mg mL^{-1} PAH/0.5 mg mL^{-1} $PAA]_{20}$ multilayers via an acid treatment at pH 2.1, exhibited more evidently protuberant nano-/micro-structures than those that were replicated from the multilayers with PAH/PAA concentration combinations of 1.5/2.0, 1.5/1.5, and 1.5 mg mL^{-1}/1.0 mg mL^{-1}. These results were also confirmed by the presence of nano- and micro-structured protuberances with narrower size range, as shown in the size distribution curves (Supporting information, Fig. S2**).** Particularly, these unique features are similar to the morphologies of superhydrophobic surfaces with a low surface energy and hierarchical roughness on a dual-sized scale. The water droplets placed onto the flat, 1.5/2.0, 1.5/1.5, 1.5/1.0, and 1.5 mg mL^{-1} (for PAH) /0.5 mg mL^{-1} (for PAA) -induced PDMS films displayed water contact angles of approximately 108°, 118°, 121°, 125°, and 131°, respectively (Fig. 2**e**). A relatively high water contact angle on the surface of the hierarchical, embossed PDMS with a nano-/micro-structure (e.g., replica from the [1.5 mg mL^{-1} PAH/0.5 mg mL^{-1} $PAA]_{20}$ films) was caused by the increase in the air trapped at the interface between the dual-sized-PDMS with a low surface energy and the water droplets [42–45]. Therefore, the hydrophobic surface could effectively restrict the formation of a moisture layer on the PDMS films or at least diminish the contact surface area between the moisture layer and the PDMS surface. Furthermore, considering that the water skin layer on the triboelectric plate dissipates the triboelectric surface charges, these phenomena suggest the possibility that the PDMS films replicated from highly nano-/micro-porous [1.5 mg mL^{-1} PAH/0.5 mg mL^{-1} $PAA]_n$ have an advantage in blocking the dramatic decrease in the triboelectric charging capacity under high humidity conditions.

Based on these results, we prepared TENGs containing Al and the replicated PDMS, which have a large polarity differences, i.e., their abilities to lose and gain electrons (Fig. 3**a**, Supporting information, Fig. S3). Herein, the Al top film was used as the contact electrode as well as the positive polarity triboelectric material. A poly(acrylate) film was glued to the top side of the bottom Al electrode, and the replicated PDMS films with a negative polarity were subsequently attached to the poly(acrylate). Additionally, four springs were affixed to the corners of the substrates for effective and periodic contact/separation of the Al and the PDMS film. The electric generation mechanism of the TENGs can be explained by the coupling between the triboelectric effect and the electrostatic induction (Supporting information, Fig. S4) [28,46–49]. When the Al contact electrode (i.e., the top electrode) and the PDMS film with an initial separation length (L_o) make physical contact via the compressive force (F_0), electrons are released from the electron-donating Al electrode to the electron-retaining PDMS film, generating triboelectric surface charges. However, when the Al and PDMS film are separated again upon the release of the compressive force, the separated surface charges produce an electric field that spans from the bottom Al electrode to the Al contact electrode, and the electric field causes a higher potential at the Al contact electrode. This potential difference induces the flow of electrons from the bottom electrode to the contact electrode and generates a potential drop that removes the tribocharge-based potential. When the separation length between the Al electrode and the PDMS film returns to the initial length (L_o), the positive charges on the Al contact electrode are fully screened and generates the same number of positive tribocharges on the bottom electrode. However, when the gap length re-decreases due to external force, a reversed polarity potential difference occurs, causing a reverse flow of electrons to neutralize the positive charges from the bottom electrode.

Furthermore, to examine the effect of the PDMS surface on the electric output performance of the LbL assembly-induced TENGs (i.e., LbL-TENGs), we prepared LbL-TENGs using PDMS replicas with different morphological sizes: (I) [1.5 mg mL^{-1} PAH/2.0 mg mL^{-1} $PAA]_{20}$, (II) [1.5 mg mL^{-1} PAH/1.5 mg mL^{-1} $PAA]_{20}$, (III) [1.5 mg mL^{-1} PAH/1.0 mg mL^{-1} $PAA]_{20}$, and (IV) [1.5 mg mL^{-1} PAH/0.5 mg mL^{-1} $PAA]_{20}$ multilayer-induced TENGs with a PDMS area of 1.5 cm × 1.5 cm and an Al contact electrode area of 3 cm × 3 cm. Fig. 3**b** and **c** show the electrical output (i.e., output voltage and current density) generated by a flat TENG and the LbL-TENGs with an increasing, repeated compressive force from 10 to 90 N (applied frequency ~ 5 Hz in 20% RH). For the flat TENG, the electrical output was approximately 75 V (open-circuit voltage) and 6.1 μA cm^{-2} (short-circuit current density) at 90 N. However, under the same mechanical force, the output voltage and current density of the LbL-TENGs increased from 81 V and 8.9 μA cm^{-2} (for the [1.5 mg mL^{-1} PAH/2.0 mg mL^{-1} $PAA]_{20}$ films) to approximately 242 V and 16.2 μA cm^{-2} (for the [1.5 mg mL^{-1} PAH/0.5 mg mL^{-1} $PAA]_{20}$), respectively. In addition, the polarity-switching tests revealed that the electric output of the LbL-TENG was generated by triboelectric mechanism, not the measurement mechanism (Supporting information, Fig. S5). This good electrical performance remained stable for approximately 18,000 cycles at 5 Hz (Fig. 3**d**), and furthermore, the electric output was maintained even despite the passing of 6 weeks after the long-term cycling test (Supporting information, Fig. S6).

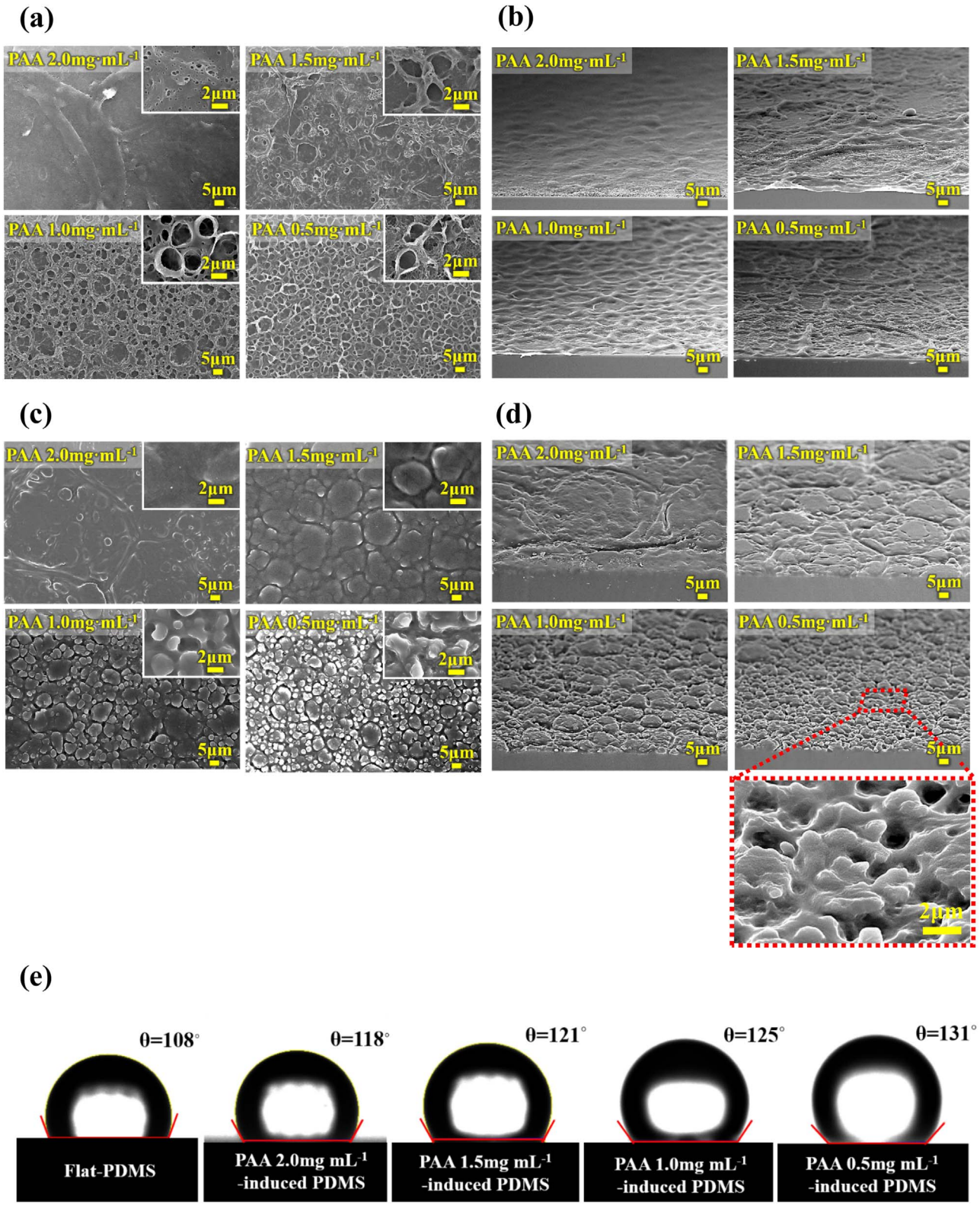

Fig. 2. (a) Top-view and (b) tilted cross-sectional FE-SEM images of porous $[PAH/PAA]_{20}$ multilayer templates prepared from four different solution concentrations of PAA (2, 1.5, 1.0, and 0.5 mg mL^{-1}). In this case, the solution concentration of PAH and the pH value for the acid treatment were fixed at 1.5 mg mL^{-1} and 2.1, respectively. (c) Top-view and (d) tilted cross-sectional FE-SEM images of the embossed PDMS films replicated from the $[PAH/PAA]_{20}$ templates with four different porosities. (e) Static contact angles of water drops on flat, $[1.5\ mg\ mL^{-1}\ PAH/\ 2.0\ mg\ mL^{-1}\ PAA]_{20}$, $[1.5\ mg\ mL^{-1}\ PAH/1.5\ mg\ mL^{-1}\ PAA]_{20}$, $[1.5\ mg\ mL^{-1}\ PAH/1.0\ mg\ mL^{-1}\ PAA]_{20}$, $[1.5\ mg\ mL^{-1}\ PAH/0.5\ mg\ mL^{-1}\ PAA]_{20}$ template-molded PDMS films. All the LbL-assembled multilayer templates were treated with a pH 2.1 aqueous solution.

In view of energy generation mechanism, the enhanced electric output of the hierarchically embossed PDMS (particularly, PDMS with dual-sized protuberances) can be explained by the increase in the effective charging surface area and the more compressible structure of the embossed PDMS replica compared with that of the flat PDMS film under the same external force. That is, the embossed PDMS film with a

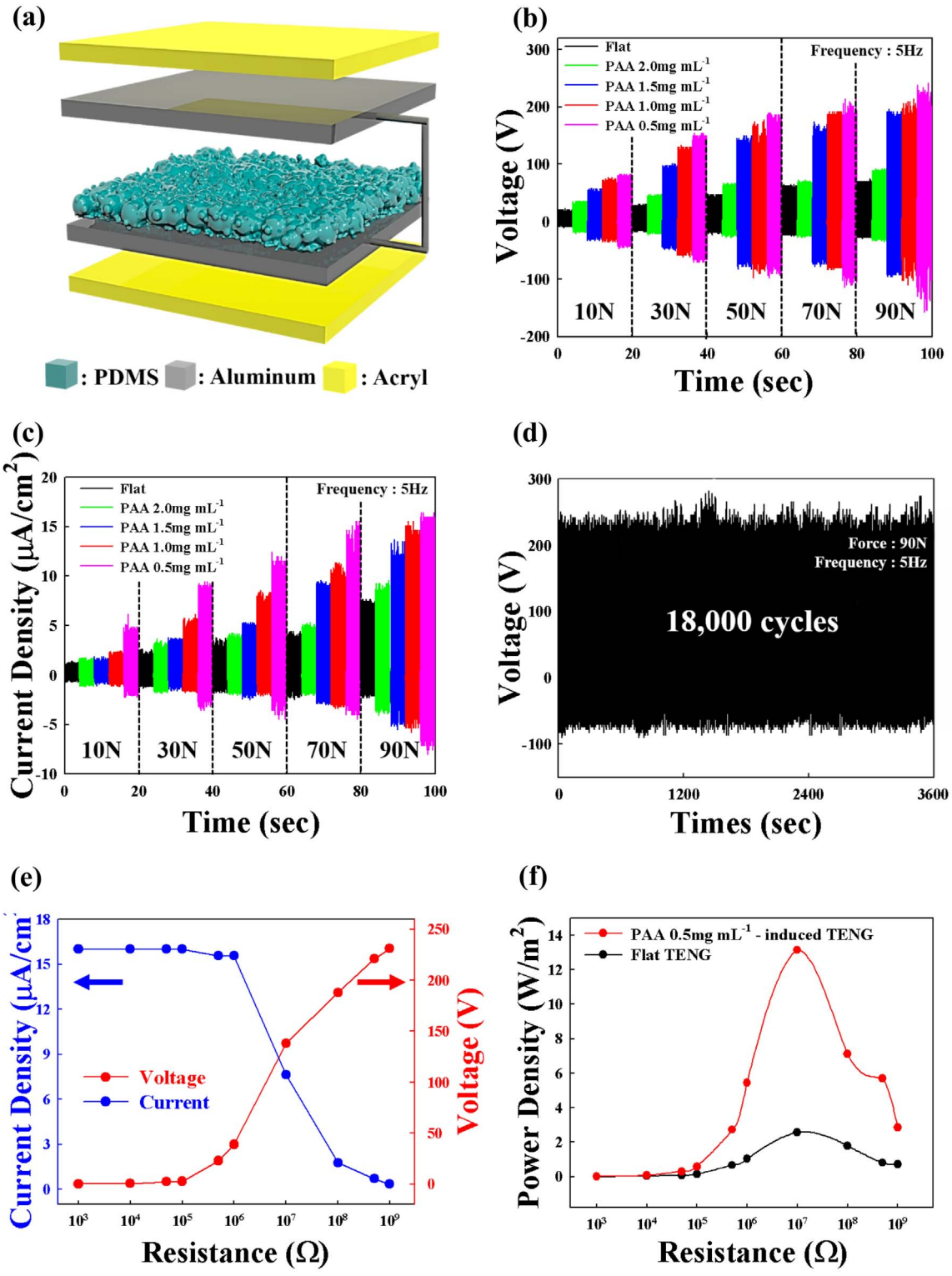

Fig. 3. (a) Schematic for LbL-TENG (b) Output voltages and (c) current densities of flat and LbL-TENGs as a function of compressive force. (d) Stability test of [1.5 mg mL^{-1} PAH/0.5 mg mL^{-1} $PAA]_{20}$-induced TENG. (e) Dependences of the output voltages and current densities on the external load resistance under the compressive force of 90 N. (f) Dependences of the power densities of flat TENG and [1.5 mg mL^{-1} PAH/0.5 mg mL^{-1} $PAA]_{20}$-induced TENG on the external load resistance under a compressive force of 90 N.

large surface area can generate a larger amount of triboelectric surface charges compared to that of the flat PDMS film under the same mechanical force. Although the embossed structure of the PDMS can obstruct the immaculate contact between the Al electrode and the PDMS under a low compressive force, an increase in the compressive force causes the elastic PDMS film with the embossed structure to readily deform, resulting in a capacitance change and a larger electrostatic induction area between the two triboelectric films (Supporting information, Fig. S7). Lee et al. reported that a porous PDMS film with a sponge structure could generate additional triboelectric charges on the surface of the inner pores via electrostatic induction and a notable capacitance change under an increased compressive force [29].

Resistors were connected as external loads to investigate the effective power of the [1.5 mg mL^{-1} PAH/0.5 mg mL^{-1} $PAA]_{20}$ film-

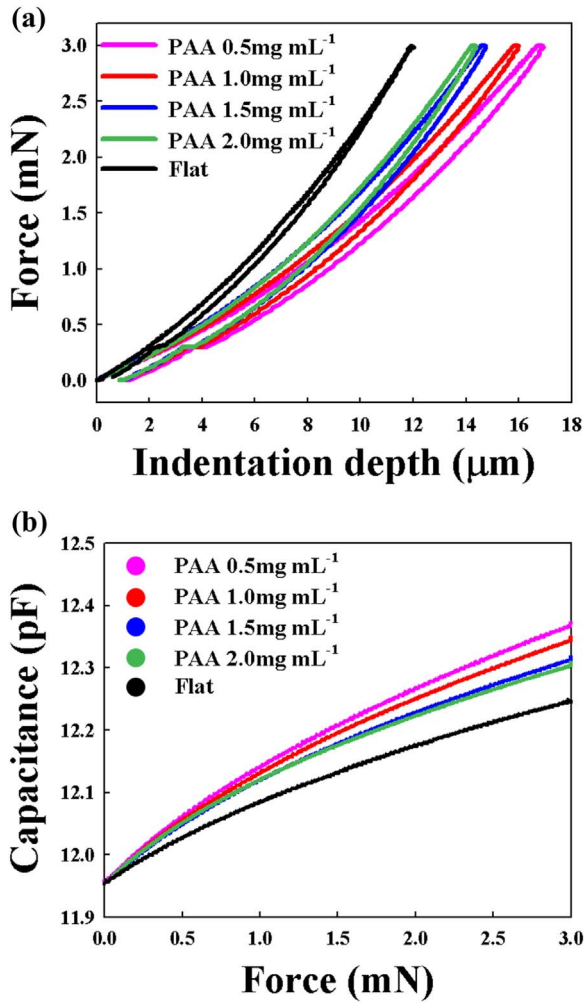

Fig. 4. (a) Force-displacement curves, (b) Force-capacitance curves of a flat PDMS film and $[PAH/PAA]_{20}$ multilayer film-induced protuberant PDMS films.

induced TENG with a dual-sized structure (Fig. 3**e**). As the load resistance increased from 10^3 to 10^9 Ω under a compressive force of 90 N, the instantaneous voltage peak increased but the current peak density decreased due to ohmic loss. As a result, the instantaneous power output reached a maximum value (i.e., $W = I_{peak}^2 R = 13.6\ W\ m^{-2}$) at an external load resistance of 10^7 Ω (Fig. 3**f**). Therefore, this LbL-TENG can be considered a current source with a large internal resistance when the external resistance load is significantly smaller than the internal resistance. These devices exhibited a 5.2-fold power enhancement compared to that of a flat PDMS-based TENG.

To better understand the relationship between the surface morphology of the PDMS and the electric output, we investigated the indentation depth displacement of the LbL-induced PDMS films using an external compressive force. Fig. 4**a** shows the force loading and unloading curves of the flat and LbL-induced PDMS films from the nanoindentation tests. The indentation depth for the flat PDMS was measured to be 12.03 μm under a maximum compressive loading force of 3 mN. However, the indentation depth of the LbL-induced PDMS films increased from 14.76 (for the $[1.5\ mg\ mL^{-1}$ PAH/$2.0\ mg\ mL^{-1}$ $PAA]_{20}$ films) to 16.96 μm (for the $[1.5\ mg\ mL^{-1}$ PAH/$0.5\ mg\ mL^{-1}$ $PAA]_{20}$ films) under the same force. Particularly, given that the capacitance is closely related to the distance between the electrodes ($C = \varepsilon_0 \varepsilon_r A/d$, where ε_0, ε_r, A, and d are the permittivity of free space ($8.854 \times 10^{-12}\ Fm^{-1}$), the relative static permittivity, the contact area, and the distance between the top and bottom electrode, respectively), the capacitance of the micro-/nano-structured PDMS film changed more with the same mechanical force, and, thus, the triboelectric charge density and output voltage can be increased (Fig. 4**b**) [50]. As a result, these phenomena qualitatively underpin the enhancement of electric output as the nano-/micro-structure of the LbL-induced PDMS films evolved, as shown in Fig. 3.

Furthermore, we examined the effects of nano-/micro-structured protuberances on the triboelectric potential of a hierarchically embossed PDMS device via analytical simulations using COMSOL multiphysics software (Fig. 5). For the convenience of the simulation, an Al contact electrode with a width of 0.5 cm and a thickness of 75 μm was placed on a PDMS film with the same shape and dimensions with a contact electrode. The separation length between the PDMS and Al electrodes was fixed at 2 mm. However, the compressive force was not considered in our simulation. The triboelectric charge density for two tribo-charged surfaces was assigned with ± 1 $\mu C \cdot m^{-2}$. In this case, the triboelectric potential of the hierarchical nano-/micro-size-embossed PDMS film significantly increased when the electrostatic induction contact and surface areas were increased, which evidently implied more charge density was generated on the nano-/micro-structured surface in comparison with that on the surfaces of the flat- and microsized-embossed PDMS films. Given that an increase in the triboelectric charge density is directly related to the difference in the triboelectric potential between the PDMS and the contact electrode as well as the increase in the transferred charges, the notable electrical performance of the LbL-TENG is closely related to the formation of the dual-sized PDMS features.

We also investigated the effect of the surface structure of the triboelectric film on the electric output of the LbL-TENGs under humid conditions (Supporting information, Fig. S8**).** As mentioned earlier, the contact angles for the water droplets on the PDMS films increased from 106° to 131° when the film surface changed from a flat to hierarchical morphology with nano-/micro-structured protuberances. Because the adsorbed water molecules on the triboelectric films act as antistatic materials inducing a significant reduction in the triboelectric charging capacity, the nano-/micro-embossed PDMS films with enhanced hydrophobic properties exhibit a high humidity-resistant electric output. Although the output voltages and current densities of all the TENGs decreased due to the dissipation of the triboelectric charges with the increasing % RH, the $[1.5\ mg\ mL^{-1}$ PAH/$0.5\ mg\ mL^{-1}$ $PAA]_{20}$ film induced-TENG exhibited the strong humidity-resistant electric output compared to other TENGs. More specifically, its output voltage and current density at 80% RH were approximately 194 V and 12.6 $\mu A\ cm^{-2}$, respectively, which implied only a 20% loss from the initial output at 20% RH (Fig. 6**a, b and** Supporting information, Fig. S9**)**. In contrast, the electric output of the flat TENG decreased from 75 V to 14 V and 8 $\mu A\ cm^{-2}$ to 1.4 $\mu A\ cm^{-2}$ (i.e., approximately 82% loss of the initial values) when the RH increased from 20% to 80%. These results demonstrate that the electrical output of the LbL-TENG with a dual-sized structure is highly resistant to humidity in comparison with that of the other TENGs based on flat or microstructured PDMS films. This high humidity-resistant electric performance is attributed to the nano-/micro-structured surface of the $[1.5\ mg\ mL^{-1}$ PAH/$0.5\ mg\ mL^{-1}$ $PAA]_{20}$ film-induced PDMS similar to the superhydrophobic surface composed of nano- and micro-sized protuberances.

To visually demonstrate the output power generated from a nano-/micro-embossed-TENG, we designed a direct-current bridge rectifying circuit composed of the $[1.5\ mg\ mL^{-1}$ PAH/$0.5\ mg\ mL^{-1}$ $PAA]_{20}$ film-induced TENG and 100 commercial LEDs without a capacitor (Supporting information, Fig. S10). When the device was pushed (with a force of 90 N) and released at 20% and 80% RH, the 100 green LEDs instantaneously turned on and off (**Video S1**). However, the output power generated from the flat TENGs at 80% RH was not sufficient to illuminate the 100 green LEDs (Fig. 6**c**). These results show that the increase in the hydrophobicity of the triboelectric surface minimizes the electric output loss of TENG from the dissipation of triboelectric charges under high humidity conditions.

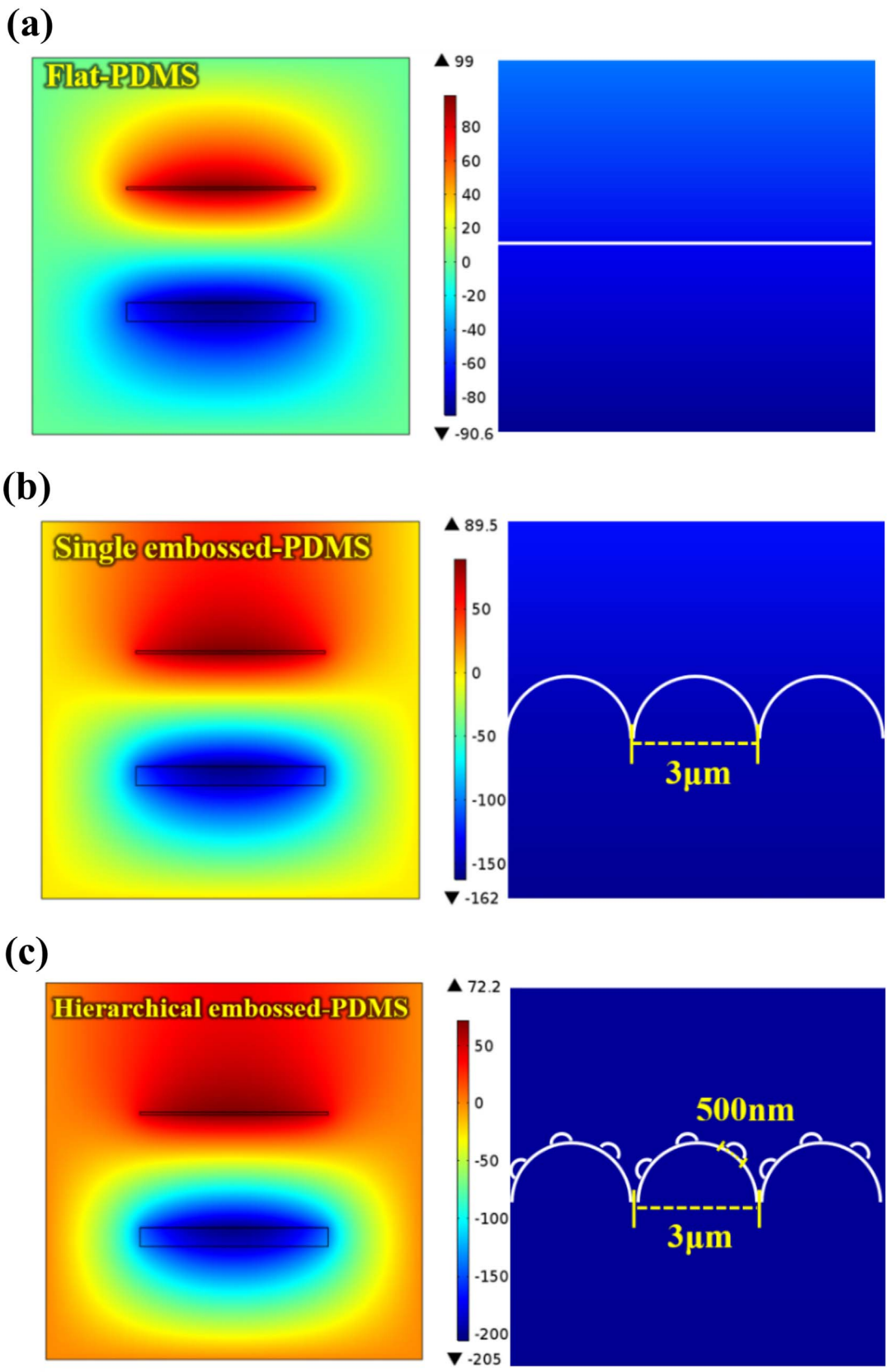

Fig. 5. Simulation of the triboelectric potential distribution between the contact electrode and PDMS ((a) flat, (b) microstructure, and (c) nano-/micro-structure) using the COMSOL multiphysics software.

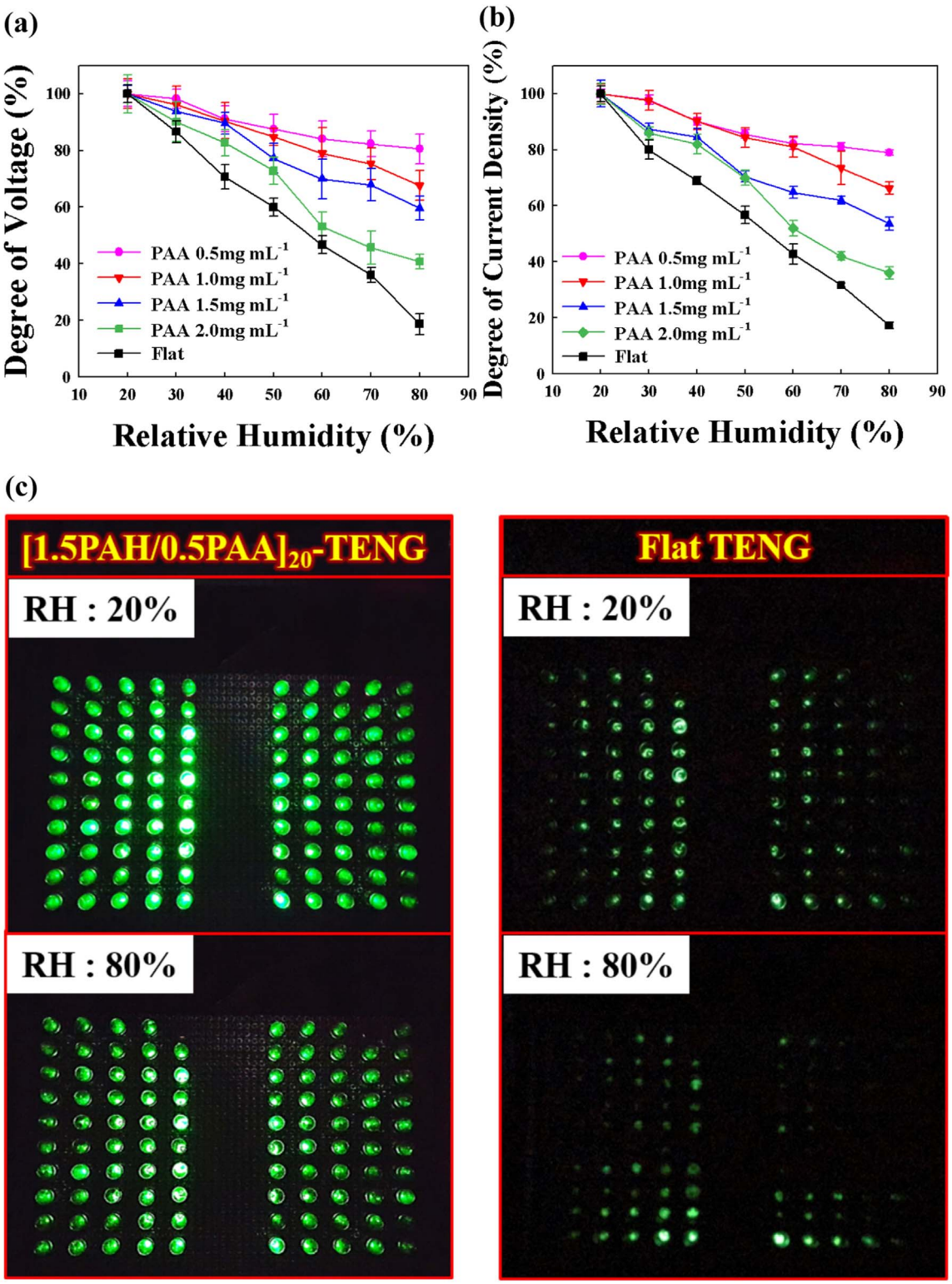

Fig. 6. The degree of the (a) output voltages and (b) current densities for the flat PDMS, and four different LbL-TENGs as a function of the RH. (c) Photographic images of the TENG measurement apparatus and 100 green LEDs illuminated by the [1.5 mg mL^{-1} PAH/0.5 mg mL^{-1} PAA]$_{20}$-induced TENG in a humidity-controlled environment.

For further enhancing the electrical outputs and the humidity resistance of LbL-TENGs, fluorination treatment was additionally introduced into the surface of nano-/micro-embossed PDMS. Song et al. reported that the formation of fluorinated self-assembled monolayer (SAM) onto flat PDMS could transfer larger amounts of electrons from Al to modified PDMS compared to those induced by pristine PDMS during triboelectric contact with Al electrode [51]. Therefore, in the case of depositing FOTS onto the [1.5 mg mL^{-1} PAH/0.5 mg mL^{-1} PAA]$_{20}$ film-induced PDMS (shortly, fluorinated LbL-PDMS), the voltage output and current density of the resultant TENG were increased up to 288 V and 17 μA cm^{-2} under a compressive force of 90 N, respectively. (Fig. 7**a and** Supporting information, Fig. S11a). We also observed the relative stable electric performance of fluorinated LbL-TENG with slight degradation of voltage output for 18,000 cycles

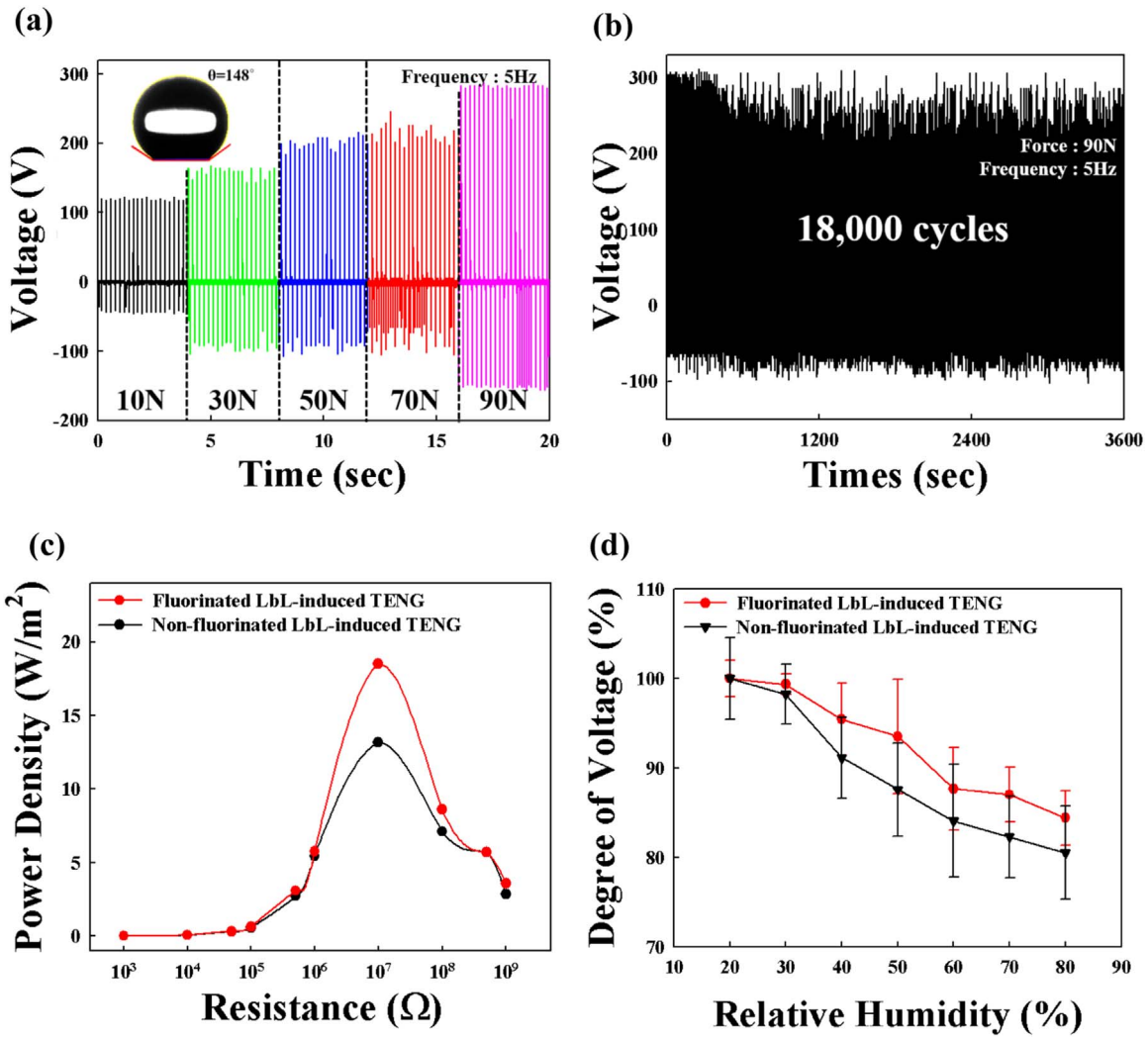

Fig. 7. (a) Voltage output and (b) stability tests of LbL-TENG composed of fluorinated [1.5 mg mL^{-1} PAH/0.5 mg mL^{-1} PAA]$_{20}$-induced PDMS replica and Al electrode. (c) Dependences of the power densities of fluorinated and non-fluorinated LbL-TENGs on the external load resistance. (d) Degree of voltages of fluorinated and non-fluorinated LbL-TENGs as a function of RH. In this case, the PDMS plates used for fluorinated and non-fluorinated LbL-TENGs were replicated from [1.5 mg mL^{-1} PAH/0.5 mg mL^{-1} PAA]$_{20}$ films.

(Fig. 7**b**). Based on these results, we investigated the effective power of fluorinated LbL-TENG with increasing load resistance from 10^3 to 10^9 Ω under a compressive force of 90 N (Fig. 7**c**). Although the instantaneous electric output behavior (i.e., voltage peak and current peak density) of fluorinated LbL-TENG were almost similar with that of non-fluorinated LbL-TENG (i.e., [1.5 mg mL^{-1} PAH/0.5 mg mL^{-1} PAA]$_{20}$ film-induced TENG) (Supporting information, Fig. S11b), the effective power output of fluorinated LbL-TENG notably increased up to 18.5 W m^{-2}. In addition to high electronegative property of FOTS, extremely low surface energy of FOTS can generate the more improved humid-resistant electric performance than that obtained from the LbL-TENG without fluorination treatment. First, the water droplet angle of fluorinated LbL-PDMS with nano-/micro-embossed structure was approximately 147°, which almost reached the contact angle corresponding to superhydrophobic surface. Additionally, considering that water droplets onto the fluorinated PDMS surface grow more slowly maintaining relatively high water contact angle compared to those onto the flat or the dual structure-sized PDMS without fluorination treatment in excess saturated vapor phase (Supporting information, Figs. S12 and S13), we envision the possibility that the fluorinated LbL-PDMS with dual-sized structure can prevent a significant reduction in the triboelectric charging capacity under high humidity condition. On the basis of these results, the electric output of fluorinated LbL-TENG was investigated as a function of % RH. In this case, its output voltage and current density at 80% RH were measured to be approximately 242 V and 14.2 μA cm^{-2}, respectively, which exhibited only a 16% loss from the initial output at 20% RH (Fig. 7**d**, Supporting information, Fig. S14). As a result, the dual-sized structural morphology and low surface energy effectively prevented the formation of a water skin layer, which dissipates the triboelectric charge capacity, and minimized the interface area between the water layer and the fluorine-modified PDMS triboelectric film.

4. Conclusion

We demonstrated that the LbL assembly-modulated hierarchical surface structure of PDMS with fluorination treatment can be effectively used for the preparation of TENGs with high humidity-resistant electric outputs. In particular, controlling the PE concentration and using an acid treatment for the PAH/PAA multilayers significantly increased the degree of hydrophobicity and the charging surface area of the PDMS replica films because of the formation of nano-/micro-sized protuberances. Additionally, the fluorination treatment of hierarchical PDMS surface further increased the triboelectric polarities between PDMS plate and Al electrode, mimicking superhydrophobic surface, which allowed high and stable electric outputs from TENGs under a wide range of humidity conditions. Given that these porous, LbL-assembled multilayer films can be easily prepared on various substrates

irrespective of the substrate size and shape, we believe that our approach can offer a novel path for the design of high-performance TENGs with scalable size via a simple and facile preparation methodology.

Acknowledgement

This work was supported by the National Research Foundation (NRF) grant funded by the Korean government (NRF-2015R1A2A1A01004354).

Appendix A. Supporting information

Supplementary data associated with this article can be found in the online version at http://dx.doi.org/10.1016/j.nanoen.2017.12.001.

References

[1] F.R. Fan, L. Lin, G. Zhu, W.Z. Wu, R. Zhang, Z.L. Wang, Transparent triboelectric nanogenerators and self-powered pressure sensors based on micropatterned plastic films, Nano Lett. 12 (2012) 3109–3114.
[2] S.H. Wang, L. Lin, Z.L. Wang, Nanoscale triboelectric-effect-enabled energy conversion for sustainably powering portable electronics, Nano Lett. 12 (2012) 6339–6346.
[3] Z.L. Wang, G. Zhu, Y. Yang, S.H. Wang, C.F. Pan, Progress in nanogenerators for portable electronics, Mater. Today 15 (2012) 532–543.
[4] F.R. Fan, Z.Q. Tian, Z.L. Wang, Flexible triboelectric generator!, Nano Energy 1 (2012) 328–334.
[5] E.R. Post, K. Waal, Electrostatic Power Harvesting in Textiles, Proceedings of the E. S.A. Annual Meeting on Electrostatics, Paper G1, 2010.
[6] U. Khan, T.H. Kim, H. Ryu, W. Seung, S.W. Kim, Graphene tribotronics for electronic skin and touch screen applications, Adv. Mater. 29 (2017) 1603544.
[7] J.H. Park, K.J. Park, T. Jiang, Q.J. Sun, J.H. Huh, Z.L. Wang, S. Lee, J.H. Cho, Light-transformable and -healable triboelectric nanogenerators, Nano Energy 38 (2017) 413–418.
[8] H.Y. Guo, M.H. Yeh, Y.C. Lai, Y.L. Zi, C.S. Wu, Z. Wen, C.G. Hu, Z.L. Wang, All-in-one shape-adaptive self-charging power package for wearable electronics, ACS Nano 10 (2016) 10580–10588.
[9] K. Zhao, Z.L. Wang, Y. Yang, Self-powered wireless smart sensor node enabled by an ultrastable, highly efficient, and superhydrophobic-surface-based triboelectric nanogenerator, ACS Nano 10 (2016) 9044–9052.
[10] G. Zhu, W.Q. Yang, T.J. Zhang, Q.S. Jing, J. Chen, Y.S. Zhou, P. Bai, Z.L. Wang, Self-powered, ultrasensitive, flexible tactile sensors based on contact electrification, Nano Lett. 14 (2014) 3208–3213.
[11] J.H. Lee, R. Hinchet, S.K. Kim, S. Kim, S.W. Kim, Shape memory polymer-based self-healing triboelectric nanogenerator, Energy Environ. Sci. 8 (2015) 3605–3613.
[12] H.Y. Guo, J. Chen, L. Tian, Q. Leng, Y. Xi, C.G. Hu, Airflow-induced triboelectric nanogenerator as a self-powerd sensor for detecting humidity and air flow rate, ACS Appl. Mater. Interfaces 6 (2014) 17184–17189.
[13] Z.L. Wang, J. Chen, L. Lin, Progress in triboelectric nanogenerators as a new energy technology and self-powered sensors, Energy Environ. Sci. 8 (2015) 2250–2282.
[14] S.M. Li, W.B. Peng, J. Wang, L. Lin, Y.L. Zi, G. Zhang, Z.L. Wang, All-elastomer-based triboelectric nanogenerator as a keyboard cover to harvest typing energy, ACS Nano 10 (2016) 7973–7981.
[15] G.L. Liu, H.Y. Guo, L. Chen, X. Wang, D.P. Wei, C.G. Hu, Double-induced-mode integrated triboelectric nanogenerator based on spring steel to maximize space utilization, Nano Res. 9 (2016) 3355–3363.
[16] S.H. Wang, Y.N. Xie, S.M. Niu, L. Lin, Z.L. Wang, Freestanding triboelectric-layer-based nanogenerators for harvesting energy from a moving object or human motion in contact and non-contact modes, Adv. Mater. 26 (2014) 2818–2824.
[17] M.L. Seol, J.H. Woo, D.I. Lee, H. Im, J. Hur, Y.K. Choi, Nature-replicated nano-in-micro structures for triboelectric energy harvesting, Small 10 (2014) 3887–3894.
[18] C.K. Jeong, K.M. Baek, S.M. Niu, T.W. Nam, Y.H. Hur, D.Y. Park, G.T. Hwang, M. Byun, Z.L. Wang, Y.S. Jung, K.J. Lee, Topographically-designed triboelectric nanogenerator via block copolymer self-assembly, Nano Lett. 14 (2014) 7031–7038.
[19] B. Dudem, Y.H. Ko, J.W. Leem, S.H. Lee, J.S. Yu, Highly transparent and flexible triboelectric nanogenerators with subwavelength-architectured polydimethylsiloxane by a nanoporous anodic aluminum oxide template, ACS Appl. Mater. Interfaces 7 (2015) 20520–20529.
[20] J.M. Wu, C.K. Chang, Y.T. Chang, High-output current density of the triboelectric nanogenerator made from recycling rice husks, Nano Energy 19 (2016) 39–47.
[21] S.H. Shin, Y.E. Bae, H.K. Moon, J. Kim, S.H. Choi, Y. Kim, H.J. Yoon, M.H. Lee, J. Nah, Formation of triboelectric series via atomic-level surface functionalization for triboelectric energy harvesting, ACS Nano 11 (2017) 6131–6138.
[22] W. Seung, M.K. Gupta, K.Y. Lee, K.S. Shin, J.H. Lee, T.Y. Kim, S. Kim, J. Lin, J.H. Kim, S.W. Kim, Nanopatterned textile-based wearable triboelectric nanogenerator, ACS Nano 9 (2015) 3501–3509.
[23] Z.H. Lin, G. Zhu, Y.S. Zhou, Y. Yang, P. Bai, J. Chen, Z.L. Wang, A. Self-Powered Triboelectric, Nanosensor for mercury ion detection, Angew. Chem. Int. Ed. 52 (2013) 5065–5069.
[24] D. Jang, Y. Kim, T.Y. Kim, K. Koh, U. Jeong, J. Cho, Force-assembled triboelectric nanogenerator with high-humidity-resistant electricity generation using hierarchical surface morphology, Nano Energy 20 (2016) 283–293.
[25] G. Zhu, Z.H. Lin, Q.S. Jing, P. Bai, C.F. Pan, Y. Yang, Y.S. Zhou, Z.L. Wang, Toward large-scale energy harvesting by a nanoparticle-enhanced triboelectric nanogenerator, Nano Lett. 13 (2013) 847–853.
[26] G. Zhu, C.F. Pan, W.X. Guo, C.Y. Chen, Y.S. Zhou, R.M. Yu, Z.L. Wang, Triboelectric-generator-driven pulse electrodeposition for micropatterning, Nano Lett. 12 (2012) 4960–4965.
[27] V. Nguyen, R.S. Yang, Effect of humidity and pressure on the triboelectric nanogenerator, Nano Energy 2 (2013) 604–608.
[28] B. Dudem, Y. Ko, J. Leem, J. Lim, J. Yu, Hybrid energy cell with hierarchical nano/micro-architectured polymer film to harvest mechanical, solar, and wind energies individually/simultaneously, ACS Appl. Mater. Interfaces 8 (2016) 30165–30175.
[29] K.Y. Lee, J. Chun, J.H. Lee, K.N. Kim, N.R. Kang, J.Y. Kim, M.H. Kim, K.S. Shin, M.K. Gupta, J.M. Baik, S.W. Kim, Hydrophobic sponge structure-based triboelectric nanogenerator, Adv. Mater. 26 (2014) 5037–5042.
[30] Y.F. Huang, Y.J. Jen, L.C. Chen, K.H. Chen, S. Chattopadhyay, Design for approaching cicada-wing reflectance in low- and high-index biomimetic nanostructures, ACS Nano 9 (2015) 301–311.
[31] Y. Kim, K.Y. Lee, S.K. Hwang, C. Park, S.W. Kim, J. Cho, Layer-by-layer controlled perovskite nanocomposite thin films for piezoelectric nanogenerators, Adv. Funct. Mater. 24 (2014) 6262–6269.
[32] M. Park, Y. Kim, Y. Ko, S. Cheong, S.W. Ryu, J. Cho, Amphiphilic layer-by-layer assembly overcoming solvent polarity between aqueous and nonpolar media, J. Am. Chem. Soc. 136 (2014) 17213–17223.
[33] S. Cheong, J.K. Kim, J. Cho, Functional nanocomposites with perfect nanoblending between water-soluble polymers and hydrophobic inorganic nanoparticles: applications to electric-stimuli-responsive films, Nanoscale 8 (2016) 18315–18325.
[34] D. Kim, S. Cheong, Y.G. Ahn, S.W. Ryu, J.K. Kim, J. Cho, Multicatalytic colloids with highly scalable, adjustable, and stable functionalities in organic and aqueous media, Nanoscale 8 (2016) 7000–7016.
[35] D. Kim, Y. Kim, J. Cho, Solvent-free nanocomposite colloidal fluids with highly integrated and tailored functionalities: rheological, ionic conduction, and magneto-optical properties, Chem. Mater. 25 (2013) 3834–3843.
[36] Y. Ko, H. Baek, Y. Kim, M. Yoon, J. Cho, Hydrophobic nanoparticle-based nanocomposite films using In situ ligand exchange layer-by-layer assembly and their nonvolatile memory applications, ACS Nano 7 (2013) 143–153.
[37] Y. Ko, D. Shin, B. Koo, S.W. Lee, W.S. Yoon, J. Cho, Ultrathin supercapacitor electrodes with high volumetric capacitance and stability using direct covalent-bonding between pseudocapacitive nanoparticles and conducting materials, Nano Energy 12 (2015) 612–625.
[38] J.D. Mendelsohn, C.J. Barrett, V.V. Chan, A.J. Pal, A.M. Mayes, M.F. Rubner, Fabrication of microporous thin films from polyelectrolyte multilayers, Langmuir 16 (2000) 5017–5023.
[39] L. Zhai, F.C. Cebeci, R.E. Cohen, M.F. Rubner, Stable superhydrophobic coatings from polyelectrolyte multilayers, Nano Lett. 4 (2004) 1349–1353.
[40] J. Choi, M.F. Rubner, Influence of the degree of ionization on weak polyelectrolyte multilayer assembly, Macromolecules 38 (2005) 116–124.
[41] S.S. Shiratori, M.F. Rubner, pH-dependent thickness behavior of sequentially adsorbed layers of weak polyelectrolytes, Macromolecules 33 (2000) 4213–4219.
[42] B. Cortese, S. D'Amone, M. Manca, I. Viola, R. Cingolani, G. Gigli, Superhydrophobicity due to the hierarchical scale roughness of PDMS surfaces, Langmuir 24 (2008) 2712–2718.
[43] D.S. Kim, B.K. Lee, J. Yeo, M.J. Choi, W. Yang, T.H. Kwon, Fabrication of PDMS micro/nano hybrid surface for increasing hydrophobicity, Microelectron. Eng. 86 (2009) 1375–1378.
[44] M.M. Stanton, R.E. Ducker, J.C. MacDonald, C.R. Lambert, W.G. McGimpsey, Superhydrophobic, highly adhesive, polydimethylsiloxane (PDMS) surfaces, J. Colloid Interface Sci. 367 (2012) 502–508.
[45] G. Davaasuren, C.V. Ngo, H.S. Oh, D.M. Chun, Geometric study of transparent superhydrophobic surfaces of molded and grid patterned polydimethylsiloxane (PDMS), Appl. Surf. Sci. 314 (2014) 530–536.
[46] Y.J. Fan, X.S. Meng, H.Y. Li, S.Y. Kuang, L. Zhang, Y. Wu, Z.L. Wang, G. Zhu, Stretchable porous carbon nanotube-elastomer hybrid nanocomposite for harvesting mechanical energy, Adv. Mater. 29 (2017) 1603115.
[47] K.N. Kim, J. Chun, J.W. Kim, K.Y. Lee, J.U. Park, S.W. Kim, Z.L. Wang, J.M. Baik, Highly stretchable 2D fabrics for wearable triboelectric nanogenerator under harsh environments, ACS Nano 9 (2015) 6394–6400.
[48] J.S. Chun, B.U. Ye, J.W. Lee, D. Choi, C.Y. Kang, S.W. Kim, Z.L. Wang, J.M. Baik, Boosted output performance of triboelectric nanogenerator via electric double layer effect, Nat. Commun. 7 (2016) 12985.
[49] T. Jiang, Y.Y. Yao, L. Xu, L.M. Zhang, T.X. Xiao, Z.L. Wang, Spring-assisted triboelectric nanogenerator for efficiently harvesting water wave energy, Nano Energy 31 (2017) 560–567.
[50] S.M. Niu, S.H. Wang, L. Lin, Y. Liu, Y.S. Zhou, Y.F. Hu, Z.L. Wang, Theoretical study of contact-mode triboelectric nanogenerators as an effective power source, Energy Environ. Sci. 6 (2013) 3576–3583.
[51] G. Song, Y. Kim, S. Yu, M.-O. Kim, S. –H. Park, S.M. Cho, D.B. Velusamy, S.H. Cho, K.L. Kim, J. Kim, E. Kim, C. Park, Molecularly engineered surface triboelectric nanogenerator by self-assembled monolayers (METS), Chem. Mater. 27 (2015) 4749–4755.

Dojin Kim is a M.S. candidate under Prof. Jinhan Cho at Department of Chemical and Biological Engineering in Korea University. Currently, his research interest has focused on fabrication of nano-/micro-patterned triboelectric materials and applications for energy harvesting.

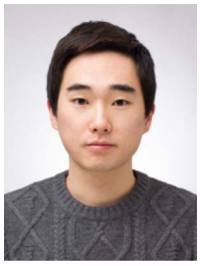

Seokmin Lee is a Ph.D. candidate under Prof. Jinhan Cho at Department of Chemical and Biological Engineering in Korea University. Currently, his research interest has focused on LbL-assembled porous elastic electrodes for triboelectric energy harvesting.

Dr. Yongmin Ko is a senior researcher at Department of Chemical and Biological Engineering in Korea University. Dr. Ko has expertise in LbL-assembled energy storage devices using layer-by-layer assembly. Currently, his research interest has focused on energy harvesting and storage devices using organic/inorganic multilayer structure.

Dr. Cheong Hoon Kwon is a senior researcher at Department of Chemical and Biological Engineering in Korea University. Dr. Kwon has expertise in the surface modification of metal or metal oxide nanoparticles for electrochemical sensors, fuel cells, and energy harvesting/storage devices. Dr. Kwon has now focused on various energy harvesting systems using metal nanoparticle-based assembly.

Dr. Jinhan Cho is a professor at the Department of Chemical & Biological Engineering in Korea University. Prof. Cho has expertise in the surface modification of metal or metal oxide nanoparticles as well as the layer-by-layer assembled functional multilayers including optical films, nonvolatile memory devices, electrochemical sensors, energy harvesting/storage devices. Prof. Cho has now focused on interface modification and piezoelectric/triboelectric properties of various energy harvesting materials using layer-by-layer assembly.